
Towards Compositional Adversarial Robustness: Generalizing Adversarial Training to Composite Semantic Perturbations

Yun-Yun Tsai¹ Lei Hsiung² Pin-Yu Chen³ Tsung-Yi Ho²

Abstract

Model robustness against adversarial examples of single perturbation type such as the ℓ_p -norm has been widely studied, yet its generalization to more realistic scenarios involving multiple semantic perturbations and their composition remains largely unexplored. In this paper, we firstly propose a novel method for generating composite adversarial examples. By utilizing component-wise projected gradient descent and automatic attack-order scheduling, our method can find the optimal attack composition. We then propose **generalized adversarial training (GAT)** to extend model robustness from ℓ_p -norm to composite semantic perturbations, such as the combination of Hue, Saturation, Brightness, Contrast, and Rotation. The results on ImageNet and CIFAR-10 datasets show that GAT can be robust not only to any single attack but also to any combination of multiple attacks. GAT also outperforms baseline ℓ_∞ -norm bounded adversarial training approaches by a significant margin.

1. Introduction

Deep neural networks have shown remarkable success in a wide variety of machine learning (ML) applications, ranging from biometric authentication (e.g., facial image recognition), medical diagnosis (e.g., CT lung cancer detection) to autonomous driving systems (traffic sign classification), etc. While these models can achieve great performance on benign data points, recent researches have shown that state-of-the-art models can be easily fooled by malicious data points crafted intentionally with adversarial perturbations (Szegedy et al., 2014).

To date, the most effective defense mechanism is to incorpo-

rate adversarial examples during model training, known as adversarial training (AT) (Madry et al., 2018; Zhang et al., 2019). Nonetheless, current adversarial training methods may not be practical because they typically consider single perturbation type (i.e., threat model) bounded by a specific distance metric (e.g., ℓ_2 -norm, ℓ_∞ -norm, etc.), which may overlook the compositional adversarial robustness against a combination of multiple threats models, such as simultaneous composite adversarial perturbations using ℓ_p -norm and semantic perturbations (e.g., hue, saturation, rotation, brightness, and contrast).

To tackle this issue, in this paper we propose **generalized adversarial training (GAT)**, which can harden against a wide range of threat models, from single ℓ_∞ -norm or semantic perturbation to a combination of them. Notably, extending standard adversarial training to composite adversarial perturbations is a challenging and non-trivial task, as each perturbation type is sequentially applied and thus the attack order will affect the effectiveness of the composite adversarial example. To bridge this gap, we propose an efficient attack order scheduling algorithm to learn the optimal ordering of various perturbation types, which will then be incorporated into the GAT framework.

Different from existing works, this paper aims to address the following questions: (a) How to generalize adversarial training from single threat model to multiple? (b) How to optimize the perturbation order from a set of semantic and ℓ_p -norm perturbations? (c) Can GAT outperform other adversarial training baselines against composite perturbations?

Our main contributions in this paper provide affirmative answers to the aforementioned fundamental questions:

1. We propose composite adversarial attack (CAA), a novel and unified approach to generate adversarial examples across from multiple perturbation types with attack-order-scheduling, including semantic perturbations (*Hue, Saturation, Contrast, Brightness and Contrast*) and ℓ_p -norm space. To the best of our knowledge, this paper is the first work that leverages scheduling algorithm for finding the optimal attack order in composite adversarial attacks.

¹Columbia University ²National Tsing Hua University, Hsinchu, Taiwan ³IBM Research. Correspondence to: Yun-Yun Tsai <yt2781@columbia.edu>, Lei Hsiung <hschung@m109.nthu.edu.tw>, Pin-Yu Chen <pin-yu.chen@ibm.com>, Tsung-Yi Ho <tyho@cs.nthu.edu.tw>.

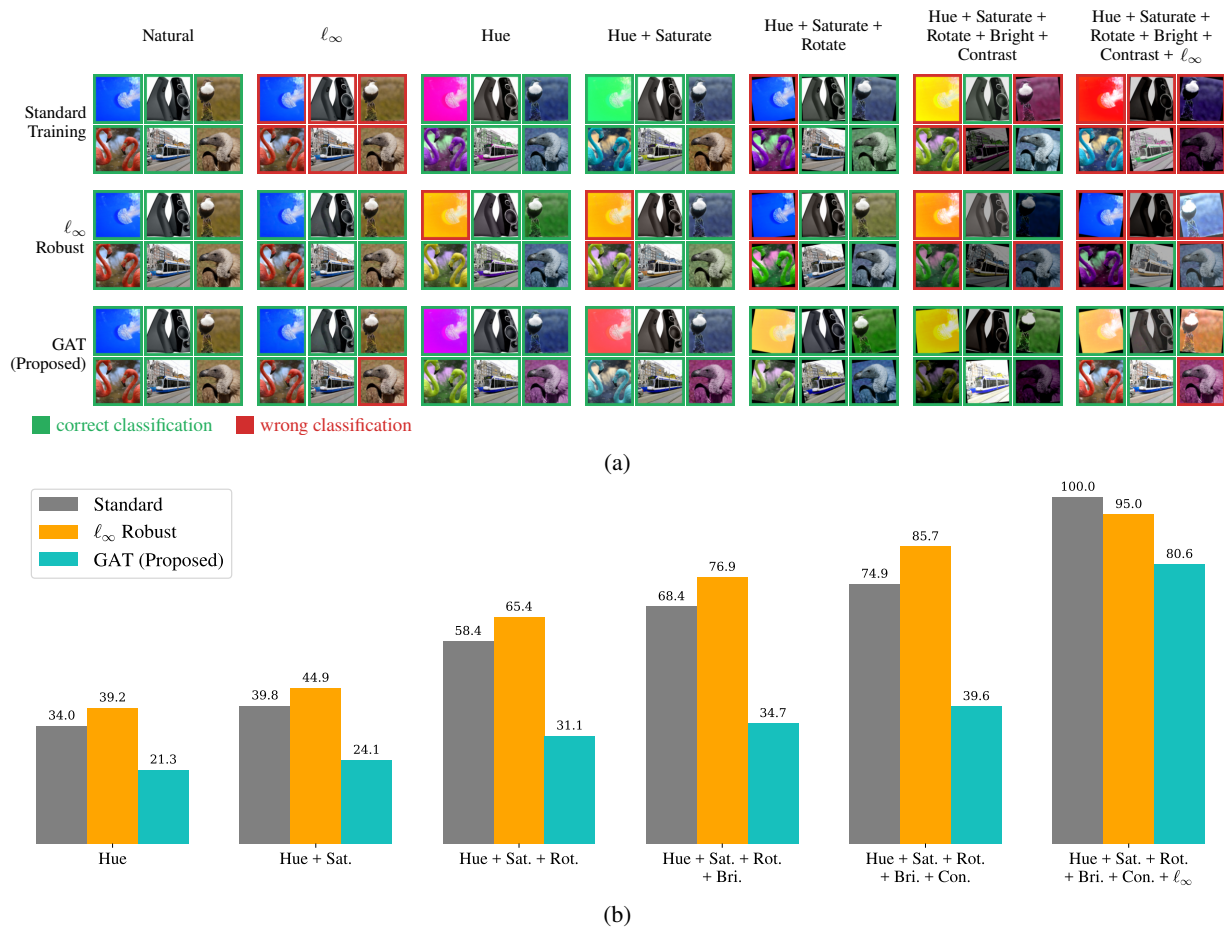


Figure 1. (a) **Qualitative study:** illustration of some perturbed examples generated by different attack combinations and their predictions by different ResNet50 models (He et al., 2016) on ImageNet, including standard training, Madry ℓ_∞ robust training (Madry et al., 2018) and our proposed GAT. The results show that our proposed GAT can maintain relatively high robust accuracy when under composite adversarial attack. (b) **Quantitative study:** the attack success rate (ASR, %) of above-mentioned models under multiple composite attacks (higher ASR means less robust) on all correctly classified test samples for each model. The attack parameters and robust accuracy (RA) are given in Tables 1 and 6.

- Building upon our composite adversarial attack framework, we propose generalized adversarial training (GAT) toward achieving compositional adversarial robustness, which enables the training of neural networks robust to composite adversarial attacks.
- For the attack part, our proposed composite adversarial attack exhibits a high attack success rate (ASR) against standard or ℓ_∞ -norm robust models. Moreover, our method with learned attack order significantly outperforms random attack ordering, giving average 9% and 7% increase in ASR on CIFAR-10 and ImageNet.
- For the defense part, comparing our GAT to other adversarial training baselines (Madry et al., 2018; Zhang et al., 2019; Laidlaw et al., 2020; Zhang et al., 2020; Wu et al., 2020; Wong et al., 2020), the results show the robust accuracy of GAT outperforms them by average 30% ~ 60% on semantic attacks and 12% ~ 22% on full attacks.

To further motivate the effectiveness of our proposed GAT framework, Fig. 1 compares the performance of different models under selected attacks, ranging from a single threat to composite threats. The models include standard training, ℓ_∞ -robust training, and our proposed GAT. The results show the limitation of ℓ_∞ -robust model (Madry et al., 2018), which is robust against the same-type adversarial attack, but becomes fragile against semantic adversarial attacks and their composition. Our proposed GAT addresses this limitation by providing a novel training approach that is robust to any combination of multiple and adversarial threats.

2. Related Work

2.1. Adversarial Semantic Perturbations

Most studies on adversarial machine learning focus on generating examples that can fool a model to make the wrong prediction (Biggio & Roli, 2018). Several works have pri-

marily focused on the vulnerability of deep neural networks against ℓ_p -norm adversarial threats (Goodfellow et al., 2015; Carlini & Wagner, 2017; Chen et al., 2018; Croce & Hein, 2020). Some works consider the adversarial threats beyond ℓ_p -norm, which generally occur in natural transformation such as geometry, color, and lightness, categorized as semantic perturbations (Hosseini & Poovendran, 2018; Joshi et al., 2019; Bhattad et al., 2019a; Shamsabadi et al., 2020; Wang et al., 2021; 2020; Bhattad et al., 2019b; Kang et al., 2019; Qiu et al., 2020). In contrast to ℓ_p -norm perturbations, semantic perturbations normally lead to semantically-similar or natural-looking adversarial examples but with large differences, in ℓ_p -norm perspective. For color translation, (Hosseini & Poovendran, 2018) shows that randomly shifting the Hue and Saturation components in Hue-Saturation-Value (HSV) color space of images can dramatically decrease the accuracy of a neural network by 88%. Similar idea is proposed by (Bhattad et al., 2019b), including colorization and texture transfer attack which can either perturb gray-scale image with natural colorization or infuse texture of one image to another. For geometric transformation, (Xiao et al., 2018; Engstrom et al., 2019) target rotate transformation. The former uses coordinate-wise optimization in each pixel, which is computationally expensive. The latter proposes a simple way by parametrizing a set of tunable parameters for spatial transformation. (Wong et al., 2019) uses Wasserstein distance for generating adversarial examples beyond ℓ_p -norm. (Mohapatra et al., 2020) studies certified robustness against semantic perturbations but does not discuss adversarial training. Prior works (Qiu et al., 2020; Dunn et al., 2020; Zhou et al., 2021) exploit the context-sensitive changes to features from the input and perturb images with the corresponding feature map interpolation.

2.2. Composite Adversarial Perturbations

Inspired by the prior works (Laidlaw & Feizi, 2019; Bhattad et al., 2019a; Jordan et al., 2019), via combining different adversarial threats, the adversarial examples can be hardened. The experimental results of prior works show how to expand the perturbation space of an image and further increase the misclassification rate of neural networks. Laidlaw and Feizi (Laidlaw & Feizi, 2019) propose the ReColorAdv attack, which admit multi-functional threats to be used for perturbing every input pixel and also combine with additional ℓ_p -norm threat. Instead of changing input by adding perturbation functionally, (Mao et al., 2020) rather utilizes genetic algorithms for searching the best combination in multiple attacks that are stronger than single attack. However, they only consider searching the order of attack combination in particular norm space (i.e., ℓ_2 , ℓ_∞ and corruption semantic space), which is different from our multiple and sequential attack setting. In (Kang et al., 2019), they propose to measure model robustness with an ensemble of unforeseen

attacks from broader threat models, including JPEG, Fog, Snow, Gabor, etc. They consider the worst case over all attacks and attempt to improve model performance against these unforeseen adversarial threats.

2.3. Adversarial Training

Adversarial training (AT) is one of the most efficient ways to defend against adversarial attacks (Kurakin et al., 2017b; Madry et al., 2018; Zhang et al., 2019). Madry et al. (Madry et al., 2018) proposed to minimize the worst-case loss in a region around the input. Further, Zhang et al. (Zhang et al., 2019) make the robust boundary more smoother by considering the ratio in loss of natural input and the perturbed input. Laidlaw et al. (Laidlaw et al., 2021) expand the adversarial attack from single to broader threats via neural perceptual distance measurement to generalize the AT with perceptual adversarial examples. AT with adversarial transformations is also done in (Stutz et al., 2020; Engstrom et al., 2019).

However, most of them only target on single adversarial threat model. Specifically, as shown in Fig. 1, a robust classifier that can help defend against ℓ_∞ -norm perturbations still has low robustness to composite semantic attacks or other ℓ_q threats ($p \neq q$) (Sharma & Chen, 2018). The adversarial robustness under multiple adversarial threats has been discussed in (Tramèr & Boneh, 2019; Wang et al., 2019; Maini et al., 2020). They propose multiple-norm adversarial training, which yields models simultaneously robust against multiple ℓ_p -norm (e.g., ℓ_1 , ℓ_2 , and ℓ_∞) attacks. Nonetheless, the considered perturbations are simultaneously added to the same data sample rather than sequentially. In contrast to their works, we consider composite adversarial perturbations involving the design of attack order and extend beyond the ℓ_p -norm attacks by considering semantic perturbations.

3. Composite Adversarial Attack and Generalized Adversarial Training

In this section, we first propose the composite adversarial attack (CAA) framework (Fig. 2), and elucidate the details of our attack order scheduling algorithm. We then adopt the CAA into adversarial training, which is called generalized adversarial training (GAT). Algorithm 1 summarizes the flow of our proposed composite adversarial examples with the attack order scheduling in Sec. 3.1 and attack perturbation optimization in Sec. 3.2.

3.1. Composite Attack Formulation

Composite adversarial attacks with order auto-scheduling: Consider the case of learning to schedule the order of K sequential adversarial perturbations for generating composite adversarial examples, we formalize the problem as follows. Let $\mathcal{F} : \mathcal{X} \rightarrow \mathbb{R}^d$ be an image

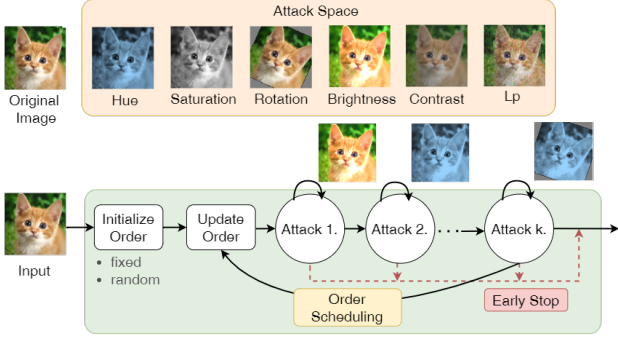


Figure 2. Pipeline of the proposed *composite adversarial attack* method. We first take an image and initialize an attack order for generating the composite semantic example. By utilizing order scheduling as mentioned in Sec. 3.1, we can dynamically optimize the attack order and iteratively update the adversarial examples.

classifier that takes any image sample $X \in \mathcal{X}$ as input and generates a d -dimensional prediction scores (e.g., softmax outputs), where d is the number of classes. Suppose there is an attack set of K perturbation types, $\Omega_A = \{A_1, \dots, A_K\}$, with a corresponding set of perturbation intervals $E = \{\epsilon_1, \epsilon_2, \dots, \epsilon_K\}$, where $\epsilon_j = [\alpha_j, \beta_j]$ governs the perturbation *boundary* in the attack space. For each attack operation $A_k \in \Omega_A$, an input X can be transformed to a perturbed sample $X_{\text{adv}} = A_k(X; \delta_k)$. Specifically, the perturbation level δ_k can be optimized through maximizing the classification error (e.g., cross-entropy loss L_{ce}) within a perturbation interval ϵ_k :

$$\arg \max_{\delta_k \in \epsilon_k} L_{ce}(\mathcal{F}(A_k(X; \delta_k)), y), \quad (1)$$

where y is the ground-truth label of X .

An optimal attack order $\omega \in \mathcal{P}_K$ can be selected from $(\Omega_A = \{A_1, \dots, A_K\}, \prec)$. Let $A_{\omega(1)}, A_{\omega(2)} \in \Omega_A$, $A_{\omega(1)} \prec A_{\omega(2)}$ denotes $A_{\omega(1)}$ strictly precedes $A_{\omega(2)}$. \mathcal{P}_K denotes the permutation polytope on K attack types and $|\mathcal{P}_K|$ grows factorially with K . Here, we formalize the order auto-scheduling as a constrained optimization problem, where the order with maximum classification error is selected by solving Eq. 2:

$$\begin{aligned} & \max_{\omega \in \mathcal{P}_K} L_{ce}(\mathcal{F}(A_{\omega(K)}(\dots A_{\omega(1)}(X; \delta_{\omega(1)}) \dots; \delta_{\omega(K)})), y), \\ & \text{s.t. } A_{\omega(m)} \prec A_{\omega(n)}, \forall m < n, m, n \in \{1, \dots, K\} \\ & \quad \delta_{\omega(k)} \in \epsilon_{\omega(k)}, \forall k \in \{1, \dots, K\} \end{aligned} \quad (2)$$

For optimization, we alternatively parameterize ω as a scheduling matrix $Z = (Z_{ij})_{i \in [K], j \in [K]}$ which is a square nonnegative real matrix. By construction, Z can be viewed as a doubly stochastic matrix, where $\sum_{i=1}^K Z_{ij} = 1, \forall j \in \{1, \dots, K\}$ and $\sum_{j=1}^K Z_{ij} = 1, \forall i \in \{1, \dots, K\}$. $Z_{ij} = 1$

means attack j is applied at time step i . We sequentially apply adversarial attacks in Ω_A according to the schedule matrix Z . The attacks in Ω_A can be reformulated as Eq. 3:

$$A(X; \{\delta_k\}_{k=1}^K) = [A_1(X; \delta_1), \dots, A_K(X; \delta_k)], \quad (3)$$

where A is a column vector of K elements $A_k(\cdot)$. the corresponding composite adversarial example $X_{\text{c-adv}}$ is formally defined as Eq. 4:

$$X_{\text{c-adv}} = Z_K A(Z_{K-1} A(\dots (Z_1 A(X; \delta) \dots; \delta); \delta), \quad (4)$$

where Z_k is the k -th row of the matrix Z and $\delta = \{\delta_k\}_{k=1}^K$. In every time step $k \in \{1, \dots, K\}$, we launch an attack indexed by Z_k and optimize the perturbation parameter δ_k within the constraint $\delta_k \in \epsilon_k$, as detailed in Sec. 3.2.

How to learn optimal attack order? Learning an optimal attack order expressed by the best scheduling matrix Z^* is originally a combinatorial optimization problem for solving the best column and row permutation of a scheduling matrix. In (Mena et al., 2018), the authors theoretically show how to extend the Sinkhorn operator (Sinkhorn, 1966) to learn and determine the optimal permutation matrix. Similarly, in our case, optimizing the attack order over a doubly stochastic matrix Z can be cast as a maximization problem, where the set of feasible solutions is convex and belongs to the Birkhoff polytope \mathcal{B} , which is the polytope of doubly stochastic matrices. To update the scheduling matrix Z , we apply the mirror descent algorithm (Wang & Banerjee, 2014). The iterative function can be formed as Eq. 5, a double-loop algorithm at iteration t is updated by

$$\begin{aligned} Z_{ij}^{t+\frac{1}{2}} &= Z_{ij}^t \exp\left(\frac{\partial L_{ce}(\cdot)}{\partial Z_{ij}^t}\right), \\ Z_{ij}^{t+1} &= \Pi_{\mathcal{B}}(Z_{ij}^{t+\frac{1}{2}}), \end{aligned} \quad (5)$$

where $\Pi_{\mathcal{B}}$ is the projection function for Z onto the Birkhoff polytope, which can be solved by Sinkhorn algorithm in a limit of iterations (Sinkhorn & Knopp, 1967). Here, we set the iteration step as 20. Our goal aims to use Z^* to approximate the optimal permutation choices P in the set \mathcal{P}_K . Specifically, we further apply a hard projection operator $\mathcal{T}(\cdot)$ on Z^* , which is a row-wise threshold. In every k -th row of the matrix Z , the operator $\mathcal{T}(\cdot)$ is defined as Eq. 6:

$$P_{kj}^* = \mathcal{T}(Z_{kj}^*) = \begin{cases} 1 & \text{if } j = \arg \max_{j' \in [K]} Z_{kj}^{*}, \\ 0 & \text{Otherwise.} \end{cases} \quad (6)$$

To correct the Birkhoff relaxation after optimization, we check whether P^* belongs to \mathcal{P}_K or not. If not, we utilize Hungarian algorithm (Kuhn, 1955; Munkres, 1957) on Z^* for solving the attack scheduling. Hungarian algorithm has cubic complexity while Sinkhorn iteration (Cuturi, 2013) has near-linear time complexity (Altschuler et al., 2017).

3.2. Component-wise Projected Gradient Descent (Comp-PGD)

Upon addressing the attack scheduling issue, we now move forward to elucidate the design of adversarial perturbation in each attack type (component) of our composite adversarial example. For most of the semantic perturbations, their parameters are of continuous value. We propose to update the parameters of semantic attacks by gradient descent algorithm with specific projection to each continuous semantic space. In particular, we show how to update the parameters in the following five different semantic perturbations, including (i) hue, (ii) saturation, (iii) brightness, (iv) contrast, and (v) rotation. We extend the iterative gradient sign method (Kurakin et al., 2017a) to optimize our semantic perturbations for T iterations, which is defined as:

$$\delta_k^{t+1} = \text{clip}_{\epsilon_k}(\delta_k^t + \alpha \cdot \text{sign}(\nabla_{\delta_k^t} J(\mathcal{F}(A_k(X; \delta_k^t)), y))), \quad (7)$$

where t denotes the iteration index, α is the step size of each iteration, $\nabla_{\delta_k^t} J(\cdot)$ is the gradient of a loss function (e.g., cross entropy) with respect to the perturbation variable δ_k^t . Let $\epsilon_k = [\alpha_k, \beta_k]$, we denote the element-wise clipping operation $\text{clip}_{\epsilon_k}(z)$ as:

$$\text{clip}_{\epsilon_k}(z) = \text{clip}_{[\alpha_k, \beta_k]}(z) = \begin{cases} \alpha_k & \text{if } z < \alpha_k, \\ z & \text{if } \alpha_k \leq z \leq \beta_k, \\ \beta_k & \text{if } \beta_k < z. \end{cases}$$

Next, We elucidate each semantic attack. The concrete examples of each of them are shown in Appendix Fig. 6.

Hue: The hue value is defined on a color wheel in HSV color space, ranging from 0 to 2π . In hue attack (A_H), we define the perturbation interval of hue as $\epsilon_H = [\alpha_H, \beta_H]$, $-\pi \leq \alpha_H \leq \beta_H \leq \pi$. Let $x_H = \text{Hue}(x)$ denote the hue value of an image x , the variation of hue value at step t is δ_H^t , and the initial variance δ_H^0 is chosen from ϵ_H uniformly. Then δ_H^t can be updated iteratively via Eq. 7, and the hue value of the perturbed image $x_{\text{adv}}^t = A_H(X; \delta_H^t)$ is:

$$x_H^t = \text{Hue}(x_{\text{adv}}^t) = \text{clip}_{[0, 2\pi]}(x_H + \delta_H^t).$$

Saturation: Similar to hue value, saturation value determines the colorfulness of an image ranging from 0 to 1. Let $x_S = \text{Sat}(x)$ denote the saturation value of an image x . If $x_S \rightarrow 0$, the image becomes more colorless, resulting in a gray-scale image if $x_S = 0$. The perturbation interval of saturation is defined as $\epsilon_S = [\alpha_S, \beta_S]$, $0 \leq \alpha_S \leq \beta_S < \infty$. Let the perturbation factor of saturation value at step t is δ_S^t , and the initial factor δ_S^0 is chosen from ϵ_S uniformly. The saturation attack is to update the perturbation factor δ_S via Eq. 7, and the saturation value of the perturbed image $x_{\text{adv}}^t = A_S(X; \delta_S^t)$ is:

$$x_S^t = \text{Sat}(x_{\text{adv}}^t) = \text{clip}_{[0, 1]}(x_S \cdot \delta_S^t).$$

Algorithm 1: Composite Adversarial Attack

Input: classifier $\mathcal{F}(\cdot)$, input x_{ori} , label y , attack space $\Omega_A = \{A_1, \dots, A_K\}$, total iteration N for order scheduling, perturbation intervals $\{\epsilon_k\}_{k=1}^K$, maximum Comp-PGD steps T

Output: Composite adversarial examples x_{adv}

```

1 # Initialization
2  $\delta_1^0, \dots, \delta_K^0 \leftarrow$  initial perturbation
3  $\omega_1 \leftarrow$  initial order (random / fixed)
4 if schedule == scheduled then
5   |  $Z_1 \leftarrow$  initial scheduling matrix by  $\omega_1$ 
6 # Iteration of attack order scheduling
7 for  $i \in \{1, \dots, N\}$  do
8   |  $x = x_{\text{ori}}$ 
9   | # Applying attacks in order
10  | for  $k \in \{1, \dots, K\}$  do
11  |   |  $A_* = A_{\omega_i(k)}$ ,  $\delta_*^0 = \delta_{\omega_i(k)}^0$ ,  $\epsilon_* = \epsilon_{\omega_i(k)}$ 
12  |   |  $x_{\text{adv}} \leftarrow A_*(x; \delta_*^0)$ 
13  |   | # Iteration of Comp-PGD
14  |   | for  $t \in \{1, \dots, T\}$  do
15  |   |   | if  $\mathcal{F}(x_{\text{adv}}) \neq y$  then
16  |   |   |   | return  $x_{\text{adv}}$  # Early stop option
17  |   |   | else
18  |   |   |   |  $\delta_*^t = \text{clip}_{\epsilon_*}(\cdot; x_{\text{adv}}; \delta_*^{t-1})$  by (7)
19  |   |   |   |  $x_{\text{adv}} \leftarrow A_*(x; \delta_*^t)$ 
20  |   |  $x = x_{\text{adv}}$ 
21  | # Resetting the attack order
22  | if schedule == random then
23  |   |  $\omega_{i+1} \leftarrow$  Shuffle a new order
24  | else if schedule == scheduled then
25  |   | # Optimize scheduling order  $Z$ 
26  |   | Evaluate  $\text{Loss}(\cdot)$  in (1) with  $\mathcal{F}(x_{\text{adv}})$  and  $y$ .
27  |   |  $Z_{i+1/2} \leftarrow Z_i * \exp(\nabla_{Z_i} \text{Loss}(\cdot))$ 
28  |   |  $Z_i \leftarrow$  Update with Sinkhorn  $\Pi_{\mathcal{B}}(Z_{i+1/2})$ 
29  |   |  $\omega_{i+1} \leftarrow$  Update the next order based on  $Z_i$ 
29  |   |   | via hard projection operator  $P^*$  in (6)
30 return  $x_{\text{adv}}$ 

```

Brightness and Contrast: Unlike hue and saturation, these values are defined on RGB color space (pixel space), and they determine the lightness, darkness, and brightness differences of images. In our implementation, we convert the images from $[0, 255]$ scale to $[0, 1]$. The perturbation interval of brightness and contrast is defined as $\epsilon_B = [\alpha_B, \beta_B]$, $-1 \leq \alpha_B \leq \beta_B \leq 1$ and $\epsilon_C = [\alpha_C, \beta_C]$, $0 \leq \alpha_C \leq \beta_C < \infty$, respectively; the same, the initial perturbation δ_B^0 and δ_C^0 are chosen from ϵ_B and ϵ_C uniformly, and can update via (7). The perturbed image x_{adv}^t under the brightness attack

(A_B) and contrast attack (A_C) can be formulated as:

$$x_{\text{adv}}^t = \text{clip}_{[0,1]}(x + \delta_B^t) \text{ and } x_{\text{adv}}^t = \text{clip}_{[0,1]}(x \cdot \delta_C^t).$$

Rotation: This transformation aims to find a rotation angle such that the rotated image has a maximum loss. The rotation implementation is constructed by (Riba et al., 2020). Given a square image x , let (i, j) denotes pixel position and (c, c) denotes the center position of x . Then the position (i', j') rotated by θ degree from (i, j) can be formulated as:

$$\begin{bmatrix} i' \\ j' \end{bmatrix} = \begin{bmatrix} \cos \theta \cdot i + \sin \theta \cdot j + (1 - \cos \theta) \cdot c - \sin \theta \cdot c \\ -\sin \theta \cdot i + \cos \theta \cdot j + \sin \theta \cdot c + (1 - \cos \theta) \cdot c \end{bmatrix}.$$

Here, we define the perturbation interval of rotation degree $\epsilon_R = [\alpha_R^\circ, \beta_R^\circ]$, $\alpha_R \leq \beta_R$, $\alpha_R, \beta_R \in \mathbb{R}$. The perturbation degree at step t is δ_R^t , and the initial degree δ_R^0 is chosen from ϵ_R uniformly. Similarly as previous attacks, the perturbation δ_R would update via Eq. 7.

3.3. Generalized Adversarial Training (GAT)

To harden the classifier against composite perturbations, we generalize the standard adversarial training approach with our proposed composite adversarial attack from Section 3.1. Our goal is to train a robust model $\mathcal{F}(\cdot)$ over a data distribution $(x, y) \sim \mathcal{D}$, and make it robust against composite perturbations in the perturbation boundary E . Existing adversarial training objectives such as the min-max loss (Madry et al., 2018) or TRADES loss (Zhang et al., 2019) can be utilized in GAT. Here we use min-max training loss (Madry’s loss) for illustration. The inner maximization in Eq. 8 is to generate $x_{c\text{-adv}}$ optimized using CAA within boundary E , and the outer minimization is for optimizing the model parameters $\theta_{\mathcal{F}}$.

$$\min_{\theta_{\mathcal{F}}} \mathbb{E}_{(x,y) \sim \mathcal{D}} \left[\max_{x_{c\text{-adv}} \in \mathcal{B}(x; \Omega_A; E)} \mathcal{L}_{ce}(\mathcal{F}(x_{c\text{-adv}}), y) \right]. \quad (8)$$

4. Experiments

In this section, we first elucidate the experimental settings and then present the performance evaluation and analysis against multiple composite attacks on two datasets: CIFAR-10 (Krizhevsky & Hinton, 2009) and ImageNet (Russakovsky et al., 2015). Additional experimental results and implementation details are shown in Appendix A.6.

4.1. Experiment Setups

Datasets: We evaluated GAT on two different datasets: CIFAR-10 (Krizhevsky & Hinton, 2009) and ImageNet (Russakovsky et al., 2015). CIFAR-10 consists of 60000 32*32 images, with 6000 images per class. There are 50000 training images and 10000 test images. ImageNet is a benchmark in image classification and object detection with 10 million images, including 1000 classes.

Attack Composition: There are many feasible combinations of threats can be utilized in the evaluation; we discuss two attack combinations here, *semantic attacks* and *full attacks*, with two scheduling strategies. Semantic attacks consist of a combination of five semantic perturbations, including *Hue*, *Saturation*, *Rotation*, *Brightness* and *Contrast* attacks. For full attacks, one can generate examples with *all five semantic attacks* and ℓ_∞ attack. We consider different order scheduling strategies: *scheduled* and *random*. That is, we can either schedule the order by the aforementioned scheduling algorithm in Section 3.1, or randomly shuffle an attack order when launching attacks for generating the corresponding composite adversarial examples.

Comparative Training Methods: We compare our GAT with several baseline adversarial training models on both datasets using two different model backbones: ResNet50 (He et al., 2016) and WideResNet34 (Zagoruyko & Komodakis, 2016b). The comparative methods are summarized in **Baseline Model Details** below. For GAT, we train our models via finetuning on the ℓ_∞ -robust pretrained model for both CIFAR-10 and ImageNet and use the min-max loss in Eq. 8 (Madry et al., 2018). Two ordering modes were adopted in GAT: random order (*GAT-f*) and scheduled order (*GAT-fs*). We also found that training from scratch using GAT is unstable due to the consideration of multiple perturbation threats (see Appendix A.2).

Baseline Model Details: We use symbols to mark the model backbones. Here, \dagger denotes models in ResNet50 (He et al., 2016) architecture and $*$ denotes models in WideResNet34 (Zagoruyko & Komodakis, 2016a). The baseline models are obtained from top-ranked models of the same architecture in RobustBench (Croce et al., 2020).

- **Normal \dagger /Normal $*$:** Standard training.
- **Madry \dagger_∞ :** ℓ_∞ adversarial training in (Madry et al., 2018).
- **Trades $*_\infty$:** ℓ_∞ adversarial training in (Zhang et al., 2019).
- **FAT \dagger_∞ :** (Zhang et al., 2020) uses friendly adversarial data that are confidently misclassified for adversarial training.
- **AWP \dagger_∞ :** (Wu et al., 2020) injects the worst-case weight perturbation during adversarial training to flatten the weight loss landscape.
- **PAT \dagger_{self} , PAT \dagger_{alex} :** Two adversarial training models based on the perceptual distance (LPIPS), two models differ: ResNet50 (*self*) and AlexNet (*alex*) (Laidlaw et al., 2020).
- **Fast-AT \dagger :** Computationally efficient ℓ_∞ adversarial training in (Wong et al., 2020).

Training & Evaluation Settings: We adopt the whole training set on both CIFAR-10 and ImageNet for model training. In every training iterative step, the images in each batch share the same attack order. Besides, the Comp-PGD is applied on each image, where we set the iteration-update step T as 10 steps of each attack component for evaluation,

and 5 steps for GAT. The perturbation interval of each attack module in GAT are specified in Table 1. During the training of GAT, we apply every attack component on the input without the *early-stopped* option to ensure the model could learn all attack components which have been launched. Furthermore, we evaluate two different order scheduling settings: *random/scheduled* during GAT on CIFAR-10. For training efficiency, we only use random order on ImageNet. As mentioned in Sec. 4.1, GAT utilizes a pre-trained model for fine-tuning to make the composite adversarial training more efficient instead of training from scratch. Different from the training phase of GAT, during the evaluation, we can trigger the *early-stop* option upon the CAA succeeds in attacking while optimizing the attack order with the scheduling algorithm mentioned in Sec. 3.1. The further discussion and comparison between different training settings of GAT, including using TRADES/Madry loss and fine-tuning/training from scratch are given in Appendix A.2.

Table 1. Perturbation interval of each attack component

	CIFAR-10	ImageNet
Hue, ϵ_H	$-\pi \sim \pi$	
Saturation, ϵ_S	$0.7 \sim 1.3$	
Rotation, ϵ_R	$-10^\circ \sim 10^\circ$	
Brightness, ϵ_B	$-0.2 \sim 0.2$	
Contrast, ϵ_C	$0.7 \sim 1.3$	
ℓ_∞, ϵ_L	8/255	4/255

Computing Resources and Code: For CIFAR-10, we train models on ResNet50 and WideResNet34 with SGD for 150 epochs. The training of GAT takes about 16 hours (ResNet50) and 28 hours (WideResNet34) on 8 Nvidia Tesla V100 GPUs. For ImageNet, we train ResNet50 with SGD for 100 epochs and about three days on 64 GPUs. The implementation is built with PyTorch (Paszke et al., 2019).

Evaluation Metrics: We report the models’ Clean and Robust Accuracy (RA, %) in Tables 2, 3, 4 and 5 against multiple composite adversarial attacks. The RA aims to evaluate the model accuracy toward the fraction of perturbed examples retrieved from the test set which is correctly classified.

4.2. Performance Evaluation

The experimental results of semantic attacks and full attacks are shown in Table 2 (CIFAR-10) and Table 3 (ImageNet). On CIFAR-10, *GAT-fs* and *GAT-f* show competitive results. Both of them outperform all the other baselines. For semantic attacks, the RA increases by 50% \sim 62% on CIFAR-10, 27% \sim 35% on ImageNet. For full attacks, the RA increases by 18% \sim 27% on CIFAR-10, 10% \sim 15% on ImageNet. Also, in Tables 4 and 5, we show the RA against three multiple threats with three different combinations, our pro-

Table 2. Comparison of accuracy (%) on CIFAR-10.

Training	Clean	Semantic attacks		Full attacks	
		Rand.	Sched.	Rand.	Sched.
Normal [†]	95.3	59.6	44.8	0.0	0.0
Madry [†] _{∞}	87.0	31.3	21.6	10.9	3.9
PAT [†] _{self}	82.4	28.6	18.0	9.3	3.0
PAT [†] _{alex}	71.6	23.4	12.9	10.2	2.8
GAT-f[†]	86.5	76.0	72.7	26.3	15.8
GAT-fs[†]	82.6	71.1	67.7	31.8	21.5
Normal*	94.0	45.6	30.6	0.0	0.0
Trades* _{∞}	84.9	16.4	8.7	5.8	1.8
FAT* _{∞}	88.1	18.5	10.5	6.3	1.7
AWP* _{∞}	85.4	15.4	8.0	6.0	1.8
GAT-f*	85.4	73.8	70.3	31.9	21.7
GAT-fs*	83.2	71.0	67.2	33.1	22.8

Table 3. Comparison of accuracy (%) on ImageNet

Training	Clean	Semantic attacks		Full attacks	
		Rand.	Sched.	Rand.	Sched.
Normal [†]	76.1	30.7	19.1	0.0	0.0
Madry [†] _{∞}	62.4	14.1	9.0	7.1	3.1
Fast-AT [†]	53.8	6.2	3.5	3.3	1.2
GAT-f[†]	60.0	40.7	36.2	17.8	11.7

posed GAT keeps outperforming other baselines and show the highest robustness than others. Comparing with GAT-f, GAT-fs can obtain better RA against full attack at the cost of lower RA against semantic attacks, which suggests a trade-off between the robustness of ℓ_∞ and semantic attacks.

Besides adversarial training models, we empirically observe the RA of models with standard training have descent performance 19% \sim 30% on ImageNet data under semantic attack (without ℓ_∞ -norm attack). However, while ℓ_∞ attack is involved in full attack or in other multiple threats (see Tables 4 and 5), the models with only standard training are unable to resist these kinds of composite semantic perturbations and the RA drops dramatically to 0%.

4.3. Analysis and Visualization

Robust accuracy v.s. Number of attacks and their combinations: We conduct an ablation study to show that the number of attacks and their combinations can hugely affect the robust accuracy, which illustrates the importance of attack ordering and the new insights into robustness through our proposed composite adversarial examples. Fig. 1b already shows our model is most resilient to composite adversarial examples consisting of different number of attacks, in terms of attaining the lowest attack success rate on all samples from the test set that were originally correctly classified by each model. Table 6 further shows that as the

Table 4. Comparison of robust accuracy (%) against 3 composite adversarial attacks (CAA_3) with scheduled ordering, including 3 combinations: CAA_{3a} : (Hue, Saturation, ℓ_∞), CAA_{3b} : (Hue, Rotation, ℓ_∞), CAA_{3c} : (Brightness, Contrast, ℓ_∞), on CIFAR-10

Training	Clean	CAA_{3a}	CAA_{3b}	CAA_{3c}
Normal [†]	95.3	0.0	0.0	0.0
Madry [†] _{∞}	87.0	30.8	19.1	19.7
PAT [†] _{self}	82.4	21.1	12.5	18.4
PAT [†] _{alex}	71.6	21.1	12.5	17.2
GAT-f[†]	86.5	36.3	29.3	25.6
GAT-fs[†]	82.6	42.1	35.4	30.7
<hr/>				
Normal*	94.0	0.0	0.0	0.0
Trades* _{∞}	84.9	30.1	20.8	10.5
FAT* _{∞}	88.1	30.4	17.4	13.2
AWP* _{∞}	85.4	34.6	23.6	11.8
GAT-f*	85.4	43.6	37.8	32.3
GAT-fs*	83.2	43.8	37.8	33.4

Table 5. Comparison of robust accuracy (%) against CAA_{3a} , CAA_{3b} , and CAA_{3c} on ImageNet (same combination as Table 4)

Training	Clean	CAA_{3a}	CAA_{3b}	CAA_{3c}
Normal [†]	76.1	0.0	0.0	0.0
Madry [†] _{∞}	62.4	14.5	9.6	17.4
Fast-AT [†]	53.8	9.9	5.4	10.2
GAT-f[†]	60.0	17.7	16.9	19.1

number of attacks increases (CAA_1 to CAA_6), the RA of our proposed GAT consistently outperforms all other models. Specifically, under three to six composite attacks (CAA_3, \dots, CAA_6), GAT is higher than other baselines by 9% \sim 29%. The higher RA of Standard model (Normal) for CAA_1 and CAA_2 is merely an artifact of Normal having higher clean accuracy than robust models (see Table 5). In Tables 4 and 5, we show the effect of different combinations when the number of attacks is fixed. Comparing GAT with others on both CIFAR-10 and ImageNet, the result shows that *GAT-f* is more robust than all baselines under 3 different attacks by 9% \sim 23%. On ImageNet, *GAT-f* also outperforms those baselines. For more experimental results, including single attack, two-component attacks and Auto-attack, please refer to our Appendix A.6.

Visualization of loss landscape: To better understanding why GAT leads to great improvement, we visualize the loss landscape of single semantic attack under three different models (see Fig. 3), including standard pretrained ResNet50 (Normal[†]), ResNet50 with ℓ_∞ -robust (Madry[†] _{∞}), and our proposed GAT fine-tuned on ℓ_∞ -robust model (*GAT-f*[†]). We visualize the cross entropy loss of selected samples for every model and sweep over the semantic perturbation space as shown in Table 1. We empirically observe that GAT can lead to more smoother and lower curve (in green color)

Table 6. Comparison of RA (%) on four adversarial training approaches against six different CAAs on ImageNet. CAA_1 : (Hue), CAA_2 : (Hue, Saturation), CAA_3 : (Hue, Saturation, Rotation), CAA_4 : (Hue, Saturation, Rotation, Brightness), CAA_5 : (Hue, Saturation, Rotation, Brightness, Contrast), CAA_6 : (Hue, Saturation, Rotation, Brightness, Contrast, ℓ_∞)

Training	CAA_1	CAA_2	CAA_3	CAA_4	CAA_5	CAA_6
Normal [†]	51.1	45.9	31.7	24.1	19.1	0.0
Madry [†] _{∞}	38.6	34.5	21.6	14.4	9.0	3.1
Fast-AT [†]	28.0	24.1	12.4	6.8	3.5	1.2
GAT-f[†]	48.1	45.6	41.3	39.1	36.2	11.7

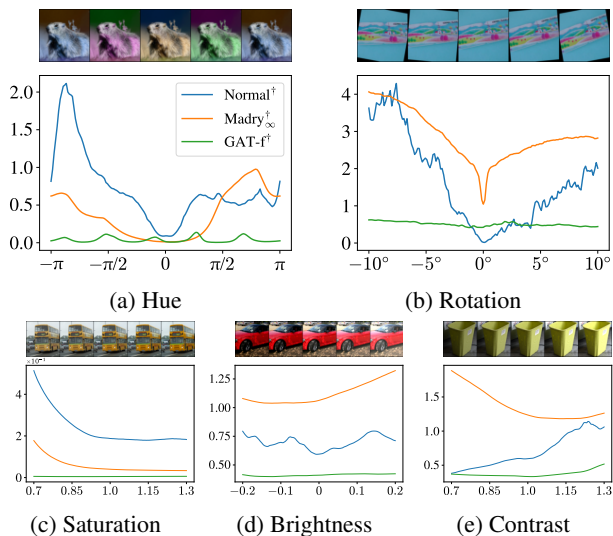


Figure 3. Loss landscape of selected examples (ImageNet) when performing specific range of five semantic attacks in different adversarial training approaches. The blue and orange color curves represent standard and ℓ_∞ robust model respectively. The green color curve represents our proposed GAT-f model

than other models on five different single semantic attacks. This phenomenon sheds light on the effectiveness of our proposed approach, which can indeed train a model robust to the composite adversarial perturbations.

5. Conclusion and Impact Statement

In this paper, we proposed GAT, a generic approach to prepare deep learning for the real world by strengthening classifiers to be robust against composite semantic perturbations. The effectiveness of GAT lies in our novel design of attack order scheduling for multiple perturbation types. Compared to existing adversarial training methods, GAT enhances robustness against a variety of adversarial perturbations, including ℓ_p norms and semantic spaces. Evaluated on CIFAR-10 and ImageNet datasets, our results demonstrate that GAT achieves the highest robust accuracy on most composite attacks by a large margin, providing new insights into achieving compositional adversarial robust-

ness. Although our end goal is to strengthen robustness via our proposed GAT and composite attacks, the attack may potentially be misused for different purposes.

References

- Altschuler, J., Weed, J., and Rigollet, P. Near-linear time approximation algorithms for optimal transport via sinkhorn iteration. *arXiv preprint arXiv:1705.09634*, 2017.
- Bhattach, A., Chong, M. J., Liang, K., Li, B., and Forsyth, D. A. Big but imperceptible adversarial perturbations via semantic manipulation. *arXiv preprint arXiv:1904.06347*, 2019a.
- Bhattach, A., Chong, M. J., Liang, K., Li, B., and Forsyth, D. A. Unrestricted adversarial examples via semantic manipulation. *arXiv preprint arXiv:1904.06347*, 2019b.
- Biggio, B. and Roli, F. Wild patterns: Ten years after the rise of adversarial machine learning. *Pattern Recognition*, 84:317–331, 2018.
- Carlini, N. and Wagner, D. Towards evaluating the robustness of neural networks. In *IEEE Symposium on Security and Privacy*, pp. 39–57, 2017.
- Chen, P.-Y., Sharma, Y., Zhang, H., Yi, J., and Hsieh, C.-J. EAD: elastic-net attacks to deep neural networks via adversarial examples. In *Proceedings of the AAAI Conference on Artificial Intelligence*, pp. 10–17, 2018.
- Croce, F. and Hein, M. Reliable evaluation of adversarial robustness with an ensemble of diverse parameter-free attacks. In *International conference on machine learning*, pp. 2206–2216. PMLR, 2020.
- Croce, F., Andriushchenko, M., Sehwag, V., Debenedetti, E., Flammarion, N., Chiang, M., Mittal, P., and Hein, M. Robustbench: a standardized adversarial robustness benchmark. *arXiv preprint arXiv:2010.09670*, 2020.
- Cuturi, M. Sinkhorn distances: Lightspeed computation of optimal transport. *Advances in neural information processing systems*, 26:2292–2300, 2013.
- Dunn, I., Hanu, L., Pouget, H., Kroening, D., and Melham, T. Evaluating robustness to context-sensitive feature perturbations of different granularities. *arXiv preprint arXiv:2001.11055*, 2020.
- Engstrom, L., Tran, B., Tsipras, D., Schmidt, L., and Madry, A. Exploring the landscape of spatial robustness. In *International Conference on Machine Learning*, pp. 1802–1811. PMLR, 2019.
- Goodfellow, I. J., Shlens, J., and Szegedy, C. Explaining and harnessing adversarial examples. *International Conference on Learning Representations*, 2015.
- He, K., Zhang, X., Ren, S., and Sun, J. Deep residual learning for image recognition. *IEEE Conference on Computer Vision and Pattern Recognition (CVPR)*, pp. 770–778, 2016.
- Hosseini, H. and Poovendran, R. Semantic adversarial examples. In *IEEE Conference on Computer Vision and Pattern Recognition Workshops*, pp. 1614–1619, 2018.
- Jordan, M., Manoj, N., Goel, S., and Dimakis, A. G. Quantifying perceptual distortion of adversarial examples. *arXiv preprint arXiv:1902.08265*, 2019.
- Joshi, A., Mukherjee, A., Sarkar, S., and Hegde, C. Semantic adversarial attacks: Parametric transformations that fool deep classifiers. In *Proceedings of the IEEE/CVF International Conference on Computer Vision*, pp. 4773–4783, 2019.
- Kang, D., Sun, Y., Hendrycks, D., Brown, T., and Steinhardt, J. Testing robustness against unforeseen adversaries. *arXiv preprint arXiv:1908.08016*, 2019.
- Krizhevsky, A. and Hinton, G. Learning multiple layers of features from tiny images. Technical Report 0, University of Toronto, Toronto, Ontario, 2009.
- Kuhn, H. W. The hungarian method for the assignment problem. *Naval research logistics quarterly*, 2(1-2):83–97, 1955.
- Kurakin, A., Goodfellow, I., and Bengio, S. Adversarial examples in the physical world. *ICLR Workshop*, 2017a.
- Kurakin, A., Goodfellow, I., and Bengio, S. Adversarial machine learning at scale. *International Conference on Learning Representations*, 2017b.
- Laidlaw, C. and Feizi, S. Functional adversarial attacks. *arXiv preprint arXiv:1906.00001*, 2019.
- Laidlaw, C., Singla, S., and Feizi, S. Perceptual adversarial robustness: Defense against unseen threat models. *arXiv preprint arXiv:2006.12655*, 2020.
- Laidlaw, C., Singla, S., and Feizi, S. Perceptual adversarial robustness: Defense against unseen threat models. In *ICLR*, 2021.
- Madry, A., Makelov, A., Schmidt, L., Tsipras, D., and Vladu, A. Towards deep learning models resistant to adversarial attacks. *International Conference on Learning Representations*, 2018.
- Maini, P., Wong, E., and Kolter, Z. Adversarial robustness against the union of multiple perturbation models. In III, H. D. and Singh, A. (eds.), *Proceedings of*

- the 37th International Conference on Machine Learning, volume 119 of *Proceedings of Machine Learning Research*, pp. 6640–6650. PMLR, 13–18 Jul 2020. URL <http://proceedings.mlr.press/v119/maini20a.html>.
- Mao, X., Chen, Y., Wang, S., Su, H., He, Y., and Xue, H. Composite adversarial attacks. *arXiv preprint arXiv:2012.05434*, 2020.
- Mena, G., Belanger, D., Linderman, S., and Snoek, J. Learning latent permutations with gumbel-sinkhorn networks. In *International Conference on Learning Representations*, 2018. URL <https://openreview.net/forum?id=Byt3oJ-0W>.
- Mohapatra, J., Weng, T.-W., Chen, P.-Y., Liu, S., and Daniel, L. Towards verifying robustness of neural networks against a family of semantic perturbations. In *Proceedings of the IEEE/CVF Conference on Computer Vision and Pattern Recognition (CVPR)*, June 2020.
- Munkres, J. R. Algorithms for the assignment and transportation problems. *Journal of The Society for Industrial and Applied Mathematics*, 10:196–210, 1957.
- Paszke, A., Gross, S., Massa, F., Lerer, A., Bradbury, J., Chanan, G., Killeen, T., Lin, Z., Gimelshein, N., Antiga, L., Desmaison, A., Kopf, A., Yang, E., DeVito, Z., Raison, M., Tejani, A., Chilamkurthy, S., Steiner, B., Fang, L., Bai, J., and Chintala, S. Pytorch: An imperative style, high-performance deep learning library. In Wallach, H., Larochelle, H., Beygelzimer, A., d'Alché-Buc, F., Fox, E., and Garnett, R. (eds.), *Advances in Neural Information Processing Systems 32*, pp. 8024–8035. Curran Associates, Inc., 2019.
- Qiu, H., Xiao, C., Yang, L., Yan, X., Lee, H., and Li, B. Semanticadv: Generating adversarial examples via attribute-conditioned image editing. In *European Conference on Computer Vision*, pp. 19–37. Springer, 2020.
- Riba, E., Mishkin, D., Ponsa, D., Rublee, E., and Bradski, G. Kornia: an open source differentiable computer vision library for pytorch. In *Proceedings of the IEEE/CVF Winter Conference on Applications of Computer Vision*, pp. 3674–3683, 2020.
- Russakovsky, O., Deng, J., Su, H., Krause, J., Satheesh, S., Ma, S., Huang, Z., Karpathy, A., Khosla, A., Bernstein, M., Berg, A. C., and Fei-Fei, L. ImageNet Large Scale Visual Recognition Challenge. *International Journal of Computer Vision (IJCV)*, 115(3):211–252, 2015. doi: 10.1007/s11263-015-0816-y.
- Shamsabadi, A. S., Sanchez-Matilla, R., and Cavallaro, A. Colorfool: Semantic adversarial colorization. In *Proceedings of the IEEE/CVF Conference on Computer Vision and Pattern Recognition*, pp. 1151–1160, 2020.
- Sharma, Y. and Chen, P.-Y. Attacking the Madry defense model with L_1 -based adversarial examples. *ICLR Workshop*, 2018.
- Sinkhorn, R. A relationship between arbitrary positive matrices and stochastic matrices. *Canadian Journal of Mathematics*, 18:303–306, 1966. doi: 10.4153/CJM-1966-033-9.
- Sinkhorn, R. and Knopp, P. Concerning nonnegative matrices and doubly stochastic matrices. *Pacific Journal of Mathematics*, 21(2):343–348, 1967.
- Stutz, D., Hein, M., and Schiele, B. Confidence-calibrated adversarial training: Generalizing to unseen attacks. In *International Conference on Machine Learning*, pp. 9155–9166. PMLR, 2020.
- Szegedy, C., Zaremba, W., Sutskever, I., Bruna, J., Erhan, D., Goodfellow, I., and Fergus, R. Intriguing properties of neural networks. *International Conference on Learning Representations*, 2014.
- Tramèr, F. and Boneh, D. Adversarial training and robustness for multiple perturbations. *arXiv preprint arXiv:1904.13000*, 2019.
- Wang, H. and Banerjee, A. Bregman alternating direction method of multipliers. In *Proceedings of the 27th International Conference on Neural Information Processing Systems - Volume 2, NIPS'14*, pp. 2816–2824, Cambridge, MA, USA, 2014. MIT Press.
- Wang, J., Zhang, T., Liu, S., Chen, P.-Y., Xu, J., Fardad, M., and Li, B. Towards a unified min-max framework for adversarial exploration and robustness. *arXiv preprint arXiv:1906.03563*, 2019.
- Wang, S., Chen, S., Chen, T., Nepal, S., Rudolph, C., and Grobler, M. Generating semantic adversarial examples via feature manipulation. *arXiv preprint arXiv:2001.02297*, 2020.
- Wang, Y., Wu, S., Jiang, W., Hao, S., Tan, Y.-a., and Zhang, Q. Demiguise attack: Crafting invisible semantic adversarial perturbations with perceptual similarity. *arXiv preprint arXiv:2107.01396*, 2021.
- Wong, E., Schmidt, F., and Kolter, Z. Wasserstein adversarial examples via projected sinkhorn iterations. In *International Conference on Machine Learning*, pp. 6808–6817. PMLR, 2019.

- Wong, E., Rice, L., and Kolter, J. Z. Fast is better than free: Revisiting adversarial training. In *International Conference on Learning Representations*, 2020. URL <https://openreview.net/forum?id=BJx040EFvH>.
- Wu, D., Xia, S.-T., and Wang, Y. Adversarial weight perturbation helps robust generalization. In *NeurIPS*, 2020.
- Xiao, C., Zhu, J.-Y., Li, B., He, W., Liu, M., and Song, D. Spatially transformed adversarial examples. *arXiv preprint arXiv:1801.02612*, 2018.
- Zagoruyko, S. and Komodakis, N. Wide residual networks. In Richard C. Wilson, E. R. H. and Smith, W. A. P. (eds.), *Proceedings of the British Machine Vision Conference (BMVC)*, pp. 87.1–87.12. BMVA Press, September 2016a. ISBN 1-901725-59-6. doi: 10.5244/C.30.87. URL <https://dx.doi.org/10.5244/C.30.87>.
- Zagoruyko, S. and Komodakis, N. Wide residual networks. *CoRR*, abs/1605.07146, 2016b. URL <http://arxiv.org/abs/1605.07146>.
- Zhang, H., Yu, Y., Jiao, J., Xing, E. P., Ghaoui, L. E., and Jordan, M. I. Theoretically principled trade-off between robustness and accuracy. In *International Conference on Machine Learning*, 2019.
- Zhang, J., Xu, X., Han, B., Niu, G., Cui, L., Sugiyama, M., and Kankanhalli, M. Attacks which do not kill training make adversarial learning stronger. In *ICML*, 2020.
- Zhou, D., Liu, T., Han, B., Wang, N., Peng, C., and Gao, X. Towards defending against adversarial examples via attack-invariant features. *ArXiv*, abs/2106.05036, 2021.

A. Appendix

A.1. Implementation Details

Training Phase In the implementation of generalized adversarial training (GAT), we consider two model architectures, ResNet-50 (He et al., 2016) and WideResNet-34 (Zagoruyko & Komodakis, 2016a), on CIFAR-10 dataset (Krizhevsky & Hinton, 2009); and ResNet-50 on ImageNet dataset (Russakovsky et al., 2015). For CIFAR-10, we set the maximum training epoch to 150 with batch size 2048, and select the model having best test accuracy for evaluation. The learning rate is set to 0.1 at the beginning and exponentially decay. We utilize the warming up learning rate technique for the first ten epochs, which means the learning rate would linearly increase from zero to the preset value (0.1) in the first ten epochs. For ImageNet, we set the maximum training epoch to 100 with batch size 1536, and select the model having best test accuracy for evaluation. The learning rate is set to 0.1 at the beginning and exponentially decay by 0.1 every 30 epochs. Similarly, we utilize the warming up learning rate technique for the first five epochs. We launch all threat models (full attacks) while training, and the attack order was randomly given in each batch. The iteration step T of each attack for Comp-PGD is set to 5, and the step size of attack A_k is set as $2.5 \cdot (\beta_k - \alpha_k)/2T$, which β_k and α_k are the values of perturbation interval defined in Table 1.

Testing Phase To compare our GAT approaches with other adversarial training baselines (Laidlaw et al., 2020; Madry et al., 2018; Zhang et al., 2019; Wong et al., 2020), we launch composite adversarial attacks (CAAs) of different number of attack types, including single attack, two attacks, three attacks, all semantic attacks, and full attacks on every robust model. The iteration step T of each attack for Comp-PGD is set as 10 and the step size is the same as training setting. The maximum iteration of order scheduling is set as 5 and we will launch the early stop option in every update step while the CAA succeeds in attacking.

A.2. Training Strategy

In our training process, we consider two training strategies: 1.) training from scratch and 2.) fine-tuning on ℓ_∞ -robust models; two learning objectives: 1.) Madry’s loss (Madry et al., 2018) and 2.) TRADES’ loss (Zhang et al., 2019). Note that $x_{c\text{-adv}} \in \mathcal{B}(x; \Omega_A; E)$ denotes the composite adversarial example $x_{c\text{-adv}}$ is perturbed by attacks from Ω_A within the perturbation intervals E . The main difference between these two is shown in Eq. 9 and Eq. 10. That is, Eq. 10 encourages the natural error to be optimized in the first term, meanwhile the robust error in the second regularization term could help minimizing the distance between the prediction of natural sample and adversarial sample; the author (Zhang et al., 2019) theoretically proved that this design of loss function could help the outputs of model to be smooth.

$$\min_{\theta_{\mathcal{F}}} \mathbb{E}_{(x,y) \sim \mathcal{D}} \left[\max_{x_{c\text{-adv}} \in \mathcal{B}(x; \Omega_A; E)} \mathcal{L}_{ce}(\mathcal{F}(x_{c\text{-adv}}), y) \right] \quad (9)$$

$$\min_{\theta_{\mathcal{F}}} \mathbb{E}_{(x,y) \sim \mathcal{D}} \left[\mathcal{L}(\mathcal{F}(x), y) + \beta \cdot \max_{x_{c\text{-adv}} \in \mathcal{B}(x; \Omega_A; E)} \mathcal{L}(\mathcal{F}(x), \mathcal{F}(x_{c\text{-adv}})) \right] \quad (10)$$

As shown in Fig. 4a, we evaluate the clean test accuracy of GAT models in every epoch with different training settings, including using two architectures (ResNet-50 / WideResNet-34), two learning objectives, and two training strategies mentioned above. We empirically find the models using fine-tuning strategy can achieve higher clean test accuracy than most of models training from scratch (see the orange, blue, red and green curve). Furthermore, we evaluate the robust test accuracy for these four models (see Fig. 4b). Under the semantic and full attacks, the models GAT- f_M (fine-tuning with Madry’s loss) achieve higher robust accuracy than GAT- f_T (fine-tuning with TRADES loss). Hence, in the section of experimental result, we focus on the model which is trained with Madry’s loss in fine-tuning setting.

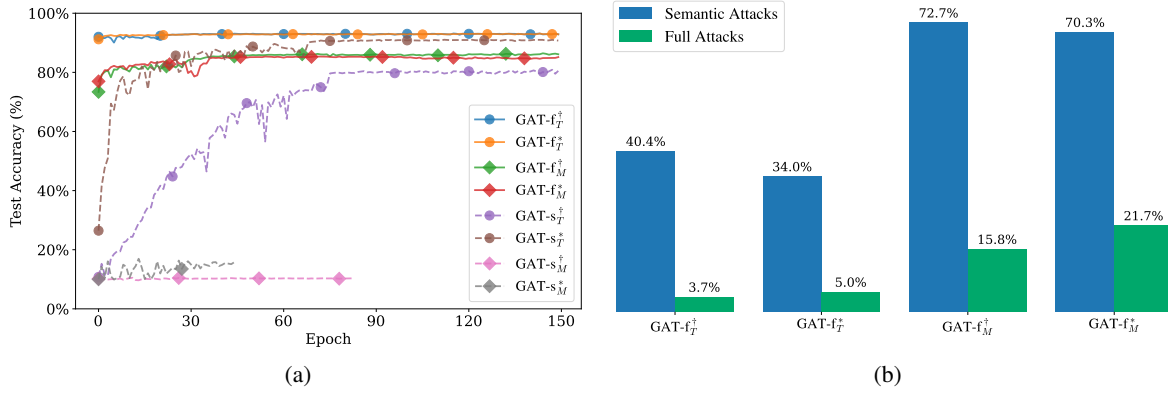


Figure 4. (a) The testing accuracy during GAT on CIFAR-10. The lower script T denotes that the model using TRADES’ loss (Zhang et al., 2019) for training, and M for Madry’s loss (Madry et al., 2018). The upper script \dagger denotes models in ResNet50 (He et al., 2016) architecture and $*$ denotes models in WideResNet34 (Zagoruyko & Komodakis, 2016a). (b) The robust accuracy (%) of our GAT fine-tuned models under semantic and full attacks.

A.3. Loss Trace Analysis of Component-wise PGD

To show the effectiveness of component-wise PGD (Comp-PGD) in Fig. 5, we visualize the update process during Comp-PGD of selected samples in CIFAR-10 when performing every single semantic attack on WideResnet-34 model. For each attack, we uniformly sample 20 start points and update δ_k using Comp-PGD by these initial points. The red margins of every sub-figure in Fig. 5 represent the margin of successfully attack by our samples. The end points of the loss trace show obviously that Comp-PGD indeed can help searching the worst case by maximizing the loss during each attack component.

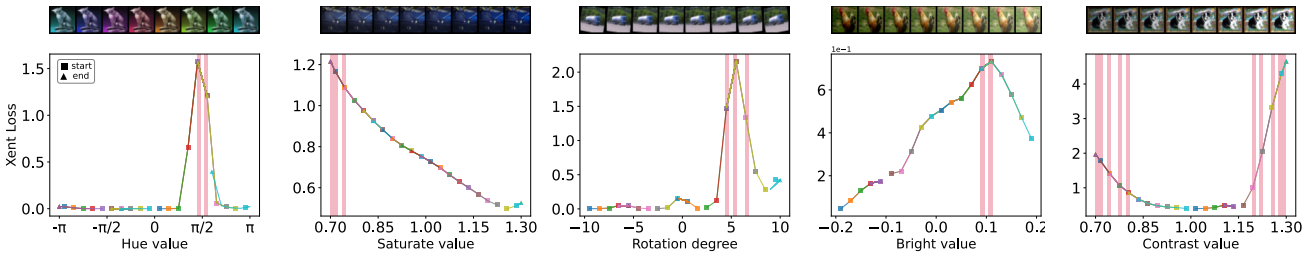


Figure 5. Component-wise PGD process of the single semantic attack.

A.4. Sensitive Analysis on Different Order of CAAs

We conduct the analysis on different *order* type under two attacks to demonstrate the influence of order on CAA. As shown in Table 7, we evaluate the attack success rate (ASR) of two attacks with different order ($\ell_\infty \rightarrow$ semantic attack / semantic attack $\rightarrow \ell_\infty$) on GAT and other baseline models. Note that ASR is the percentage of the images that can be classified correctly but be misclassified after being attacked; therefore, the lower ASR indicates the more robust model. The results show that most of baselines are more fragile to the CAA with semantic attack launched first than the attack with ℓ_∞ first. Furthermore, comparing with other models, the GAT-f model shows its robustness when attack order is changed.

Table 7. Attack success rate of two attacks with two order settings on ImageNet. The value in the parenthesis is the reduced value compare with another order settings.

Training	2 attacks (Semantic $\rightarrow \ell_\infty$)					2 attacks ($\ell_\infty \rightarrow$ Semantic)				
	Hue, ℓ_∞	Sat., ℓ_∞	Rot., ℓ_∞	Bri., ℓ_∞	Cont., ℓ_∞	ℓ_∞ , Hue	ℓ_∞ , Sat.	ℓ_∞ , Rot.	ℓ_∞ , Bri.	ℓ_∞ , Cont.
Normal [†]	100.0	99.9	100.0	99.9	99.9	99.9 (-0.1)	99.9 (-0)	99.9 (-0.1)	99.9 (-0)	99.9 (-0)
Madry [†] _{∞}	70.0	51.6	60.3	56.0	57.4	64.0 (-5.9)	48.6 (-3.1)	52.4 (-7.9)	50.4 (-5.6)	48.2 (-9.2)
Fast-AT [†]	74.7	56.0	66.5	61.7	63.0	70.8 (-3.9)	53.3 (-2.7)	59.9 (-6.5)	58.1 (-3.6)	56.0 (-7)
GAT-f[†]	63.7	58.7	60.1	59.0	63.6	61.4 (-2.3)	57.3 (-1.3)	55.5 (-4.6)	56.3 (-2.7)	56.7 (-6.9)

A.5. Examples of Single Semantic Attacks at Different Levels

Fig. 6 shows five single semantic attack with corresponding level of perturbation. Each row represents the perturbed image of a corresponding attack A_k with different perturbation values $\delta_k \in \epsilon_k$.

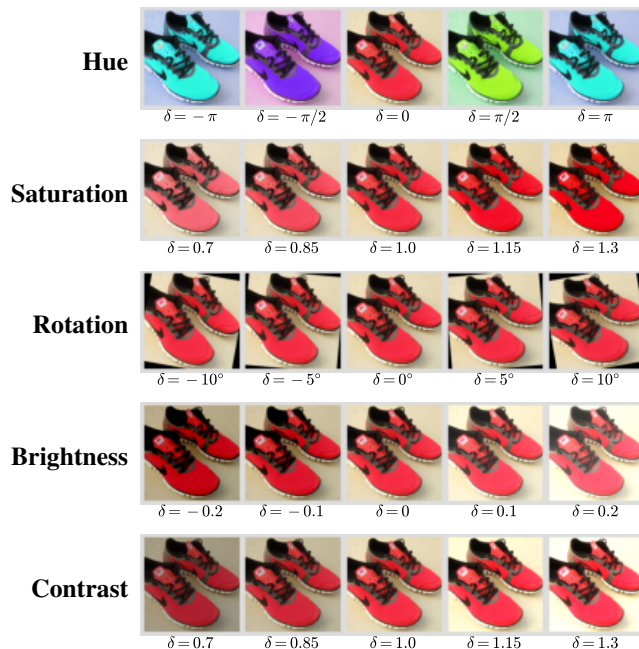


Figure 6. Single Semantic Attack Examples. Clean image was placed at the center of each row.

A.6. Additional Experimental Results and Adversarial Examples

We further evaluate multiple CAAs in this section. In Sec. A.6.1 and Sec. A.6.2, we especially show single attack on both CIFAR-10 and ImageNet. In particular, the RA of different models on single attack and their corresponding ASR are shown in Table 8, 9, 10, and 11. In Sec. A.6.3 and A.6.4, more results of multi-attacks are shown in Table 12, 13, 14 and 15.

A.6.1. SINGLE ATTACK ON CIFAR-10

Table 8. Robust accuracy of single attack, which is one of semantic attacks, on CIFAR-10

Training	Clean	Single attack					ℓ_∞ (20-step)	Auto- ℓ_∞
		Hue	Saturate	Rotation	Brightness	Contrast		
Normal [†]	95.2	81.8	93.9	88.1	92.1	93.7	0.0	0.0
Madry [†] _{∞}	87.0	70.8	84.8	79.5	77.1	79.9	53.5	49.2
PAT [†] _{self}	82.4	64.4	79.8	73.9	72.6	78.0	41.2	30.2
PAT [†] _{alex}	71.6	53.5	69.0	63.9	60.7	65.2	41.9	28.8
GAT-f [†]	86.4	85.1	84.9	82.4	84.9	84.9	40.0	34.9
GAT-fs [†]	82.6	81.3	81.2	78.9	80.5	80.5	44.8	40.5
Normal [*]	94.0	75.7	92.3	87.4	89.1	91.3	0.0	0.0
Trades [*] _{∞}	84.9	65.5	82.8	77.6	70.0	70.7	55.8	52.5
FAT [*] _{∞}	88.1	69.0	85.4	77.0	73.6	76.4	54.7	51.5
AWP [*] _{∞}	85.4	67.4	83.0	77.1	68.4	70.9	59.4	56.2
GAT-f [*]	85.4	84.0	84.0	82.0	83.3	83.3	47.3	41.9
GAT-fs [*]	83.2	81.6	81.6	79.5	80.9	80.7	47.2	42.5

Table 9. Attack success rate of single attack on CIFAR-10.

Training	Clean	Single attack						ℓ_∞ (20-step)	Auto- ℓ_∞
		Hue	Saturate	Rotation	Brightness	Contrast			
Normal [†]	0.0	14.4	1.4	8.2	3.3	1.7	100.0	100.0	
Madry [†] _{∞}	0.0	19.3	2.6	9.3	11.7	8.3	38.6	43.4	
PAT [†] _{self}	0.0	22.8	3.3	11.9	12.5	5.6	50.0	63.4	
PAT [†] _{alex}	0.0	27.5	4.2	13.0	17.0	10.0	41.4	59.8	
GAT-f [†]	0.0	2.0	1.8	5.3	1.9	1.9	53.8	59.6	
GAT-fs [†]	0.0	1.7	1.6	5.2	2.6	2.6	45.8	51.0	
Normal [*]	0.0	19.8	1.9	7.8	5.4	3.0	100.0	100.0	
Trades [*] _{∞}	0.0	23.2	2.6	9.4	17.9	16.8	34.3	38.2	
FAT [*] _{∞}	0.0	22.1	3.1	13.3	16.7	13.5	38.0	41.5	
AWP [*] _{∞}	0.0	21.8	2.9	10.5	20.2	17.3	30.4	34.2	
GAT-f [*]	0.0	1.8	1.6	4.6	2.4	2.5	44.6	50.9	
GAT-fs [*]	0.0	2.2	2.0	5.2	2.8	3.1	43.3	48.9	

A.6.2. SINGLE ATTACK ON IMAGENET

Table 10. Robust accuracy of single attack, which is one of semantic attacks, on ImageNet.

Training	Clean	Single attack						ℓ_∞ (20-step)	Auto- ℓ_∞
		Hue	Saturate	Rotation	Brightness	Contrast			
Normal [†]	76.1	51.1	72.4	67.5	68.9	71.7	0.0	0.0	
Madry [†] _{∞}	62.4	38.6	58.3	50.3	53.5	55.9	33.5	28.9	
Fast-AT [†]	53.8	28.0	48.0	38.0	42.0	43.9	27.5	24.6	
GAT-f [†]	60.0	48.1	58.1	56.2	57.6	58.0	25.2	20.9	

Table 11. Attack success rate of single attack, on ImageNet

Training	Clean	Single attack						ℓ_∞ (20-step)	Auto- ℓ_∞
		Hue	Saturate	Rotation	Brightness	Contrast			
Normal [†]	0.0	34.1	5.0	12.8	9.8	6.1	100.0	100.0	
Madry [†] _{∞}	0.0	39.2	6.8	20.9	14.8	10.9	46.3	53.6	
Fast-AT [†]	0.0	49.0	11.1	30.9	22.9	19.1	48.9	54.1	
GAT-f [†]	0.0	21.3	3.3	7.2	4.0	3.5	57.9	65.1	

A.6.3. MULTIPLE ATTACKS: 3 ATTACKS

We show the experimental results of six multi-attacks. In every multi-attack, we combine different types of three attacks from different norm spaces, including semantic space, spatial space, and ℓ_∞ space. To briefly illustrate the results in Table 12 and Table 13, we note the attack and their combinations in the following abbreviations:

- **0**: Hue, **1**: Saturate, **2**: Rotation, **3**: Brightness, **4**: Contrast, **5**: ℓ_∞ .
- **s**: scheduled order, **r**: random order.
- i.e., (0,1,5) (r) means multi-attack with Hue + Saturate + ℓ_∞ with random order.

Table 12. Attack success rate of three composite attacks on CIFAR-10.

Training	Clean	3 attacks (ℓ_∞ + two of semantic attacks)					
		(0,1,5) (r)	(0,1,5) (s)	(0,2,5) (r)	(0,2,5) (s)	(3,4,5) (r)	(3,4,5) (s)
Normal [†]	0.0	100.0	100.0	100.0	100.0	100.0	100.0
Madry [†] _{∞}	0.0	56.8	64.6	68.5	78.1	67.4	77.4
PAT [†] _{self}	0.0	65.8	74.5	75.3	84.9	68.6	77.7
PAT [†] _{alex}	0.0	60.2	70.5	70.0	82.6	65.1	76.0
GAT-f [†]	0.0	54.5	58.1	59.1	66.1	62.1	70.4
GAT-fs [†]	0.0	47.8	49.0	51.5	57.1	54.6	62.8
Normal*	0.0	100.0	100.0	100.0	100.0	100.0	100.0
Trades* _{∞}	0.0	55.6	64.6	67.0	75.5	78.1	87.6
FAT* _{∞}	0.0	57.1	65.5	75.6	85.0	70.7	80.2
AWP* _{∞}	0.0	51.5	59.5	77.9	86.2	64.5	72.4
GAT-f * [†]	0.0	46.8	48.9	51.0	55.7	55.0	62.1
GAT-fs * [†]	0.0	45.8	47.4	49.3	54.6	52.6	59.8

Table 13. Attack success rate of three composite attacks on ImageNet.

Training	Clean	3 attacks (ℓ_∞ + two of semantic attacks)					
		(0,1,5) (r)	(0,1,5) (s)	(0,2,5) (r)	(0,2,5) (s)	(3,4,5) (r)	(3,4,5) (s)
Normal [†]	0.0	100.0	100.0	100.0	100.0	99.9	100.0
Madry [†] _{∞}	0.0	69.2	76.8	62.9	72.1	76.9	84.7
Fast-AT [†]	0.0	75.6	81.6	73.3	81.1	83.9	90.0
GAT-f [†]	0.0	64.0	70.5	62.3	68.2	64.3	71.8

A.6.4. MULTIPLE ATTACKS: SEMANTIC ATTACKS AND FULL ATTACKS

We show the ASR of Semantic attacks and Full attacks in following Table 14 and 15. The RA (%) and detail of these multiple attacks have been shown in the main paper in Table 2, Table 3, and Sec. 4.2.

Table 14. Attack success rate of composite semantic attacks and composite full attacks on CIFAR-10.

Training	Clean	Semantic attacks		Full attacks	
		Random	Scheduled	Random	Scheduled
Normal [†]	0.0	37.5	53.0	100.0	100.0
Madry [†] _∞	0.0	64.1	75.2	87.5	95.5
PAT [†] _{self}	0.0	65.4	78.2	88.8	96.4
PAT [†] _{alex}	0.0	67.6	82.0	85.8	96.1
GAT-f[†]	0.0	12.1	15.9	69.6	81.8
GAT-fs[†]	0.0	13.9	18.2	61.5	73.9
Normal [*]	0.0	51.6	67.4	100.0	100.0
Trades [*] _∞	0.0	80.7	89.8	93.2	97.9
FAT [*] _∞	0.0	79.0	88.1	92.9	98.1
AWP [*] _∞	0.0	82.0	90.6	93.0	97.8
GAT-f[*]	0.0	13.6	17.6	62.6	74.6
GAT-fs[*]	0.0	14.8	19.3	60.3	72.6

Table 15. Attack success rate of composite semantic attacks and composite full attacks on ImageNet.

Training	Clean	Semantic attacks		Full attacks	
		Random	Scheduled	Random	Scheduled
Normal [†]	0.0	59.8	74.9	100.0	100.0
Madry [†] _∞	0.0	77.5	85.7	88.7	95.0
Fast-AT [†]	0.0	88.5	93.4	94.0	97.8
GAT-f[†]	0.0	32.3	39.6	70.4	80.6

A.7. Additional Visualization of Adversarial Examples under Different CAA

We provide some of the adversarial examples from CIFAR-10 in above CAAs, including single attack, two attacks, three attacks, semantic attack, and full attack. For every attack in following figures, we arrange the images into several columns; As the Fig. 7, 8, and 9 show, the left-most column represents the original images; every of the following two columns are the adversarial examples generated from one of the CAA attacks and their differences compared with the original images. Note that all of the differences have been multiplied by three for visualization purposes only.

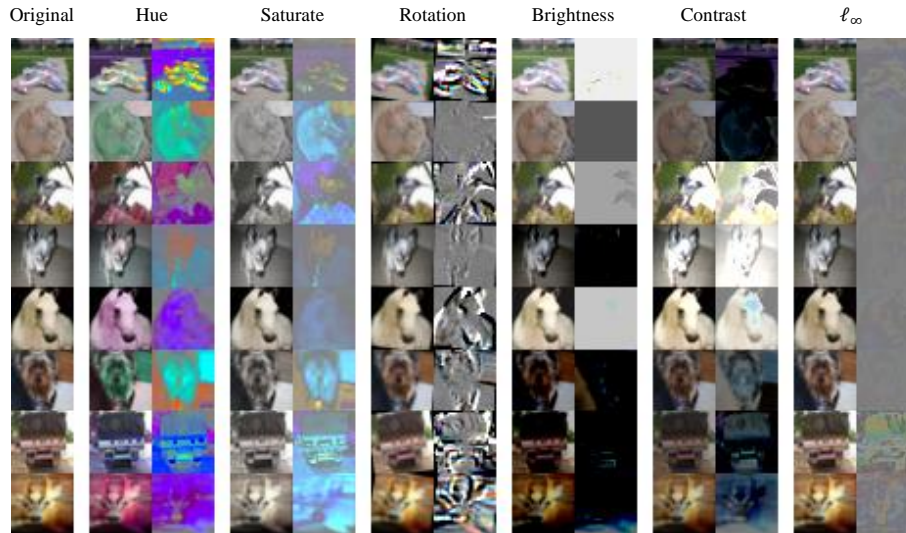


Figure 7. Adversarial examples generated under one of **single semantic** attacks (hue, saturate, rotation, bright, contrast) or ℓ_∞ attack.

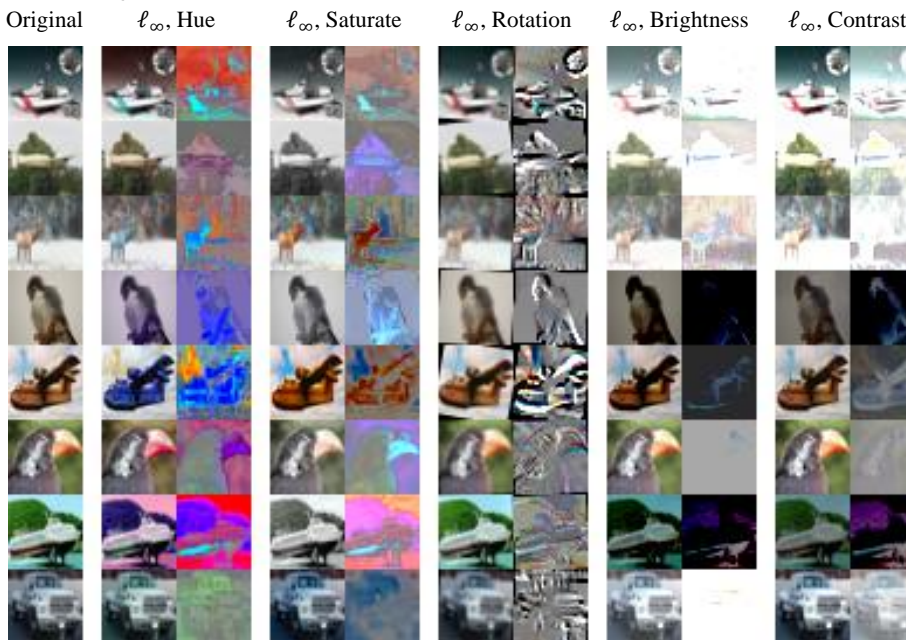


Figure 8. Adversarial examples generated under **two attacks** (composed of one semantic attack and the ℓ_∞ attack).

Generalizing Adversarial Training to Composite Semantic Perturbations

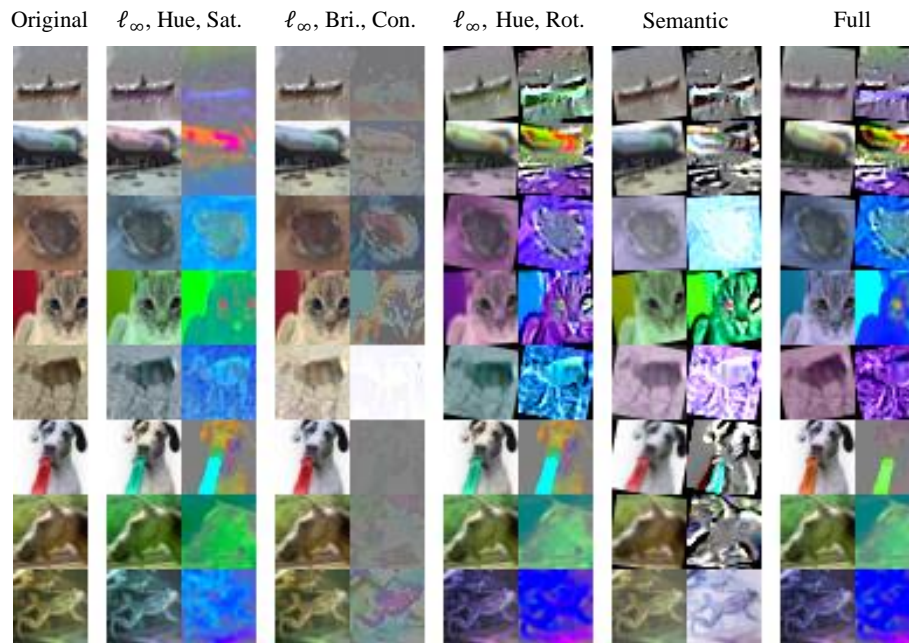


Figure 9. Adversarial examples generated under **three and other multiple attacks**. *Semantic* means we launch all semantic attacks (hue, saturate, rotation, brightness, and contrast). *Full* means we launch $\ell_\infty + \text{all semantic attacks}$.